Structure-guided evolution of antigenically distinct adeno-associated virus variants for immune evasion

Longping Victor Tse[a], Kelli A. Klinc[a], Victoria J. Madigan[a,b], Ruth M. Castellanos Rivera[a], Lindsey F. Wells[a], L. Patrick Havlik[a,b], J. Kennon Smith[c,d], Mavis Agbandje-McKenna[c,d], and Aravind Asokan[a,b,e,1]

[a]Gene Therapy Center, The University of North Carolina at Chapel Hill, Chapel Hill, NC 27599; [b]Department of Genetics, The University of North Carolina at Chapel Hill, Chapel Hill, NC; 27599; [c]Department of Biochemistry and Molecular Biology, University of Florida, Gainesville, FL 32611; [d]Center for Structural Biology, The McKnight Brain Institute, University of Florida, Gainesville, FL 32611; and [e]Department of Biochemistry and Biophysics, The University of North Carolina at Chapel Hill, Chapel Hill, NC 27599

Edited by Kenneth I. Berns, University of Florida College of Medicine, Gainesville, FL, and approved May 9, 2017 (received for review March 22, 2017)

Preexisting neutralizing antibodies (NAbs) against adeno-associated viruses (AAVs) pose a major, unresolved challenge that restricts patient enrollment in gene therapy clinical trials using recombinant AAV vectors. Structural studies suggest that despite a high degree of sequence variability, antibody recognition sites or antigenic hotspots on AAVs and other related parvoviruses might be evolutionarily conserved. To test this hypothesis, we developed a structure-guided evolution approach that does not require selective pressure exerted by NAbs. This strategy yielded highly divergent antigenic footprints that do not exist in natural AAV isolates. Specifically, synthetic variants obtained by evolving murine antigenic epitopes on an AAV serotype 1 capsid template can evade NAbs without compromising titer, transduction efficiency, or tissue tropism. One lead AAV variant generated by combining multiple evolved antigenic sites effectively evades polyclonal anti-AAV1 neutralizing sera from immunized mice and rhesus macaques. Furthermore, this variant displays robust immune evasion in nonhuman primate and human serum samples at dilution factors as high as 1:5, currently mandated by several clinical trials. Our results provide evidence that antibody recognition of AAV capsids is conserved across species. This approach can be applied to any AAV strain to evade NAbs in prospective patients for human gene therapy.

neutralizing antibody | antibody evasion | adeno-associated | gene therapy | antigenicity

Adeno-associated viruses (AAVs) are helper-dependent parvoviruses that have been established as safe and effective recombinant vectors for therapeutic gene transfer in humans. Since the approval of the first AAV1-based gene therapy in 2012, encouraging results from clinical trials involving AAV vectors for gene therapy for Leber congenital amaurosis (1), hemophilia (2), and other diseases have been reported (3). Although they use different natural AAV isolates, these gene therapy trials share the same exclusion criteria, requiring low or undetectable anti-AAV neutralizing antibody (NAb) titers in prospective patients seeking to enroll (e.g., ClinicalTrials.gov NCT01620801, NCT02618915, NCT01687608). This eligibility criterion was established owing to the high prevalence of preexisting anti-AAV NAbs in the human population arising from natural exposure; for instance, the overall prevalence of human subjects with cardiac failure positive for anti-AAV1 NAbs at titers >1:2 is ∼60%. Furthermore, most patients with high NAb titers against AAV serotype 2 also have measurable titers to AAV1, suggesting cross-reactivity between serotypes (4). Mechanistically, it is well-known that NAbs can substantially reduce gene transfer efficiency of AAV vectors by opsonization, which then accelerates clearance, alters biodistribution, blocks cell surface receptor binding, and/or adversely impacts the postattachment steps essential for efficient transduction (5, 6). Thus, the presence of preexisting anti-AAV NAbs remains a major unaddressed challenge for gene therapy (7).

Cryoelectron microscopy and 3D image reconstruction (cryoreconstruction) are powerful techniques for studying the structures of virus-antibody complexes. Although traditional methods, such as peptide scanning and site-directed mutagenesis, provided early insight into antigenic regions on the AAV capsid, cryoreconstruction has been particularly instrumental in mapping antigenic residues with high precision (8). By analyzing mixtures of antigen-binding fragments (Fabs) of purified monoclonal antibodies (mAbs) complexed with AAV capsids, cryoreconstruction has been used to resolve the antigenic footprints of various serotypes, including AAV1/6, AAV2, AAV5, and AAV8 (8–12). Those studies helped map the majority of antigenic epitopes to variable regions (VRs) on the AAV capsid surface.

Despite the diversity in amino acid sequences within the different VRs, cryoreconstruction strongly supports the idea that the number of antigenic clusters is limited and shared by different AAV strains. This attribute appears to be evolutionarily conserved, in that similar observations have been reported for the antigenic structure of other autonomous parvoviruses (13–15). However, owing to the overlap with receptor-binding footprints and other domains involved in capsid assembly, the impact of rationally modifying these antigenic epitopes on viral titer, infectivity, and tropism cannot be readily predicted. Thus, a comprehensive approach that combines structural information and directed evolution is essential to tackle this problem.

Although humoral immunity to AAV capsids has been studied in different animal models and humans (5), the relationships among the different NAb responses are not well understood. Thus, to date, most strategies evaluated to circumvent humoral immunity to AAV vectors have hinged largely on a priori assumption that antibody

Significance

Preexisting neutralizing antibodies (NAbs) against adeno-associated viruses (AAVs) pose a major, unresolved challenge that restricts patient enrollment in gene therapy clinical trials using recombinant AAV vectors. To tackle this problem, we developed a structure-guided approach to evolve AAV variants with altered antigenic footprints that cannot be recognized by preexisting antibodies. These proof-of-principle studies demonstrate that synthetic AAV variants can be evolved to evade neutralizing sera from different species—mice, nonhuman primates, and humans—without compromising yield and transduction efficiency or altering tropism. Our approach provides a roadmap for engineering any AAV strain to evade NAbs in prospective patients for human gene therapy.

Author contributions: L.V.T. and A.A. designed research; L.V.T., K.A.K., R.M.C.R., L.F.W., and L.P.H. performed research; L.V.T., V.J.M., J.K.S., and M.A.-M. contributed new reagents/analytic tools; L.V.T., V.J.M., M.A.-M., and A.A. analyzed data; and L.V.T., V.J.M., M.A.-M., and A.A. wrote the paper.

Conflict of interest statement: A.A. and M.A.-M. are cofounders of StrideBio, LLC, a company focused on commercializing AAV technologies for gene therapy and editing.

This article is a PNAS Direct Submission.

[1]To whom correspondence should be addressed. Email: aravind@med.unc.edu.

This article contains supporting information online at www.pnas.org/lookup/suppl/doi:10.1073/pnas.1704766114/-/DCSupplemental.

recognition of AAV capsids is conserved across species. Here we tested this hypothesis using AAV1 as a template, which we chose because of the availability of extensive structural information pertaining to this capsid complexed with different mAbs and its cognate glycan receptor, sialic acid (SA) (9, 10, 16). We then combined structural information from cryo-EM images of AAV1 capsids complexed with three different murine mAbs and directed evolution without selective pressure from NAbs to generate antibody-evading AAV variants. The newly evolved strains harbor synthetic antigenic footprints with highly diverse amino acid sequences that are not present in natural AAV isolates. We demonstrate that the resulting strains have the potential to evade NAbs in mouse, nonhuman primate (NHP), and human sera, thereby supporting the notion that AAV antigenicity is evolutionarily conserved among species and can be artificially evolved without affecting other capsid functions.

Results

Structural Analysis of AAV-Antibody Complexes Enables an Iterative Approach to Evolve AAV Variants. We analyzed previously resolved, cryoreconstructed structures of AAV1 capsids complexed with four different Fabs of mouse anti-AAV1 mAbs (9, 10). Annotation of the density for the Fabs onto the AAV1 capsid surface revealed that this subset of antibodies masks nearly the entire capsid surface (Fig. 1*A*). We then identified a subset of capsid surface residues (through the construction of 2D roadmap images, which pinpoint the Fab contacts on the AAV1 surface) that lie within these antigenic footprints and are implicated in direct contact with the

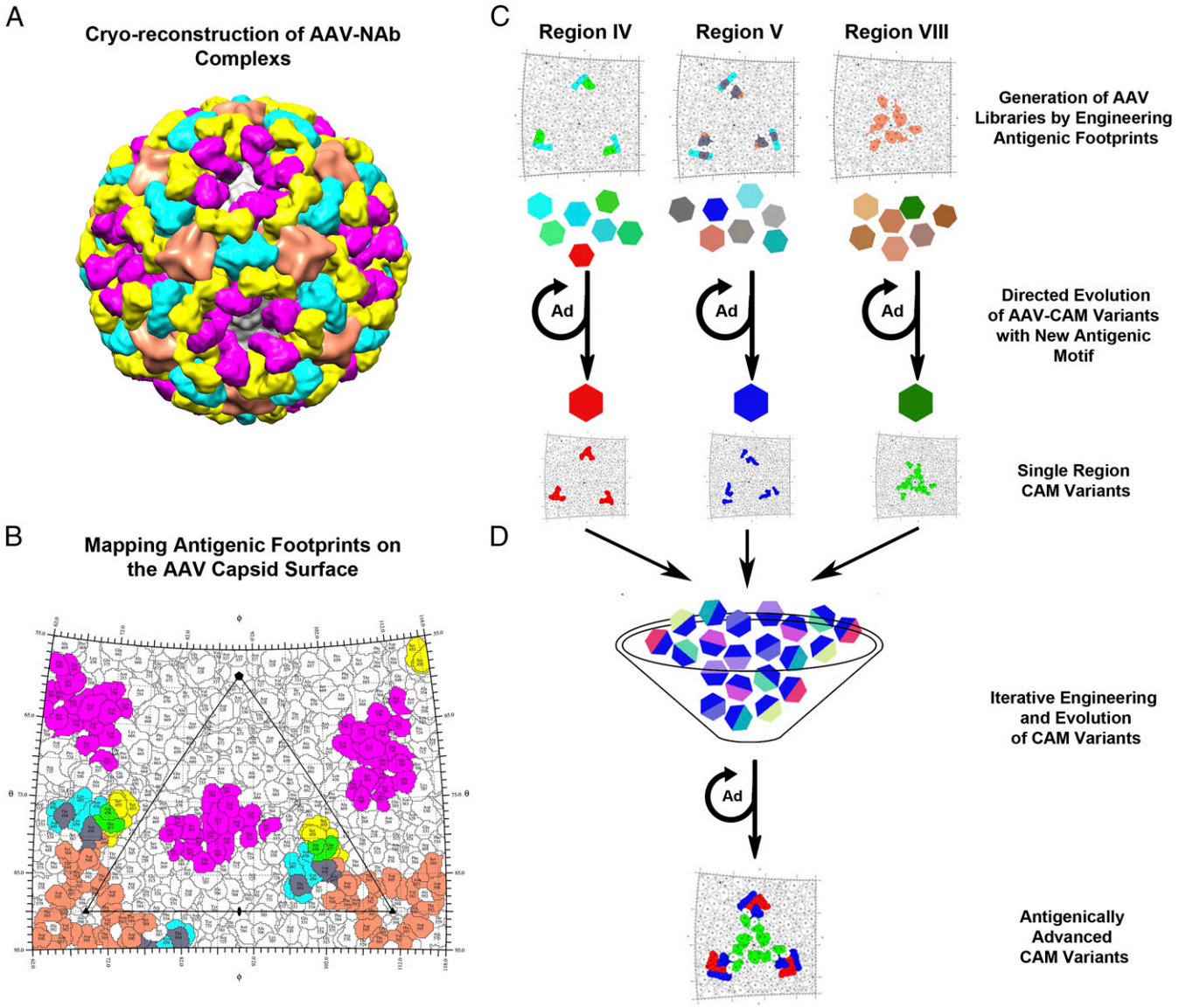

Fig. 1. Structure-guided evolution of antigenically distinct AAV variants. (*A*) A 3D model of cryoreconstructed AAV1 capsid complexed with multiple mAbs. The model depicts AAV1 complexed with the Fab densities of four different mAbs viewed along the twofold axis: ADK1a (yellow), ADK1b (magenta), 4E4 (cyan), and 5H7 (orange). (*B*) Contact residues and CAMs for four anti-AAV1 antibodies on the capsid surface in a Roadmap image generated by RIVEM (29). Color codes of each antibody are same as above; in addition, overlapping residues between antibodies are colored individually: green, ADK1a and 4E4; gray, 4E4 and 5H7. (*C*) Individual antigenic footprints on the AAV1 capsid selected for engineering and AAV library generation. Three different AAV libraries were subjected to five rounds of evolution on vascular endothelial cells coinfected with adenovirus to yield single region AAV-CAM variants. (*D*) Iterative engineering and evolution of new antigenic footprints generated from single-region AAV-CAM variants. This approach yields antigenically distinct AAV-CAM variants with footprints that have not yet emerged in nature.

different antibodies (Fig. 1*B*). Further analysis and comparison with different AAV serotypes revealed a prominent clustering of capsid antigenic footprints at the threefold symmetry axis on the capsid surface. Specifically, amino acid residues within three surface regions—region IV (456-AQNK-459), region V (492-TKTDNNNS-499), and region VIII (588-STDPATGDVH-597)—were selected for saturation mutagenesis and generation of different AAV libraries. It is important to note that the different capsid antigenic motifs (CAMs) listed above are subsets of VRs IV, V, and VIII (8). Each AAV capsid library was then subjected to five rounds of directed evolution in vascular endothelial cells, which are highly permissive to the parental AAV1 strain (Fig. 1*C*). AAV variants were identified, and combination AAV libraries were engineered using the latter as templates. Iterative rounds of evolution and capsid engineering yielded antibody-evading AAV strains characterized in the present study (Fig. 1*D*).

Antigenic Footprints on the AAV Capsid Surface Are Remarkably Plastic and Evolvable. As outlined above, the structural determined AAV region IV, V, and VIII libraries were subjected to five rounds of directed evolution. Libraries were then sequenced using the Illumina MiSeq system, with each unselected (parental) library sequenced at ~2×10^6 reads and selected (evolved) libraries sequenced at ~2×10^5 reads. Demultiplexed reads were probed for mutagenized regions of interest with a custom Perl script, with a high percentage of reads mapping to these regions for all libraries (Fig. S1*A*). At both the nucleotide and amino acid levels, all unselected libraries demonstrated high diversity and minimal bias toward any particular sequence, whereas the evolved libraries showed dramatically increased representation of one or more lead variants (Fig. 2 *A–C* and *E–G* and Fig. S1*B*). Furthermore, within the top-10 selected variants for each library, many amino acid sequences showed similarities at multiple residues (Fig. 2 *E–G*). For instance, in the evolved region V library, 97.55% of sequences spanning the mutagenized region of interest read TPGGNATR, whereas minor variants largely mimicked this sequence (Fig. 2*F*). In the case of region VIII, we observed significant enrichment (86.6%) for a variant with amino acid residues TADHDTKGV (Fig. 2*G*). The evolved region IV library demonstrated higher plasticity (QVRG, 69.57%; ERPR, 14.05%; SGGR, 3.62%), as evidenced by the range

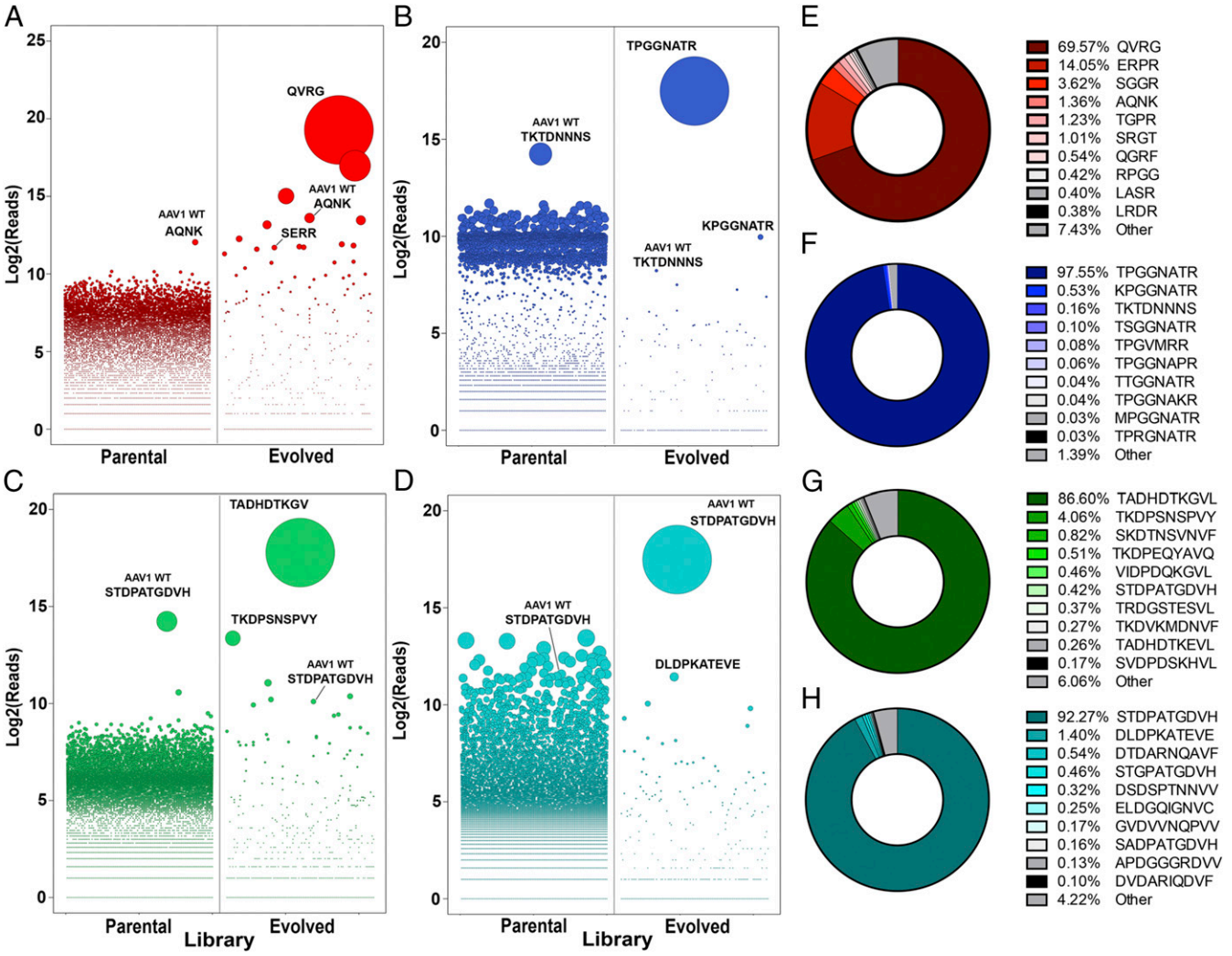

Fig. 2. Library diversity, directed evolution, and enrichment of distinct antigenic footprints. (*A–D*) Parental and evolved libraries were subjected to high-throughput sequencing using the Illumina MiSeq platform. Following analysis with a custom Perl script, enriched amino acid sequences were plotted in R for both the parental and evolved libraries of region IV (*A*), region V (*B*), region VIII (*C*), and combined regions V + VIII (*D*). Each bubble represents a distinct capsid amino acid sequence with the area proportional to the number of reads for that variant in the respective library. (*E–H*) Amino acid sequence representation was calculated for the 10 variants with the highest representation in each library after subjection to evolution. Percentages represent the number of reads for the variant in the evolved library normalized to the total number of reads containing the antigenic region of interest. "Other" sequences represent all other evolved library amino acid sequences not contained in the top-10 hits.

of amino acid residues tolerated within that antigenic region (Fig. 2*A*).

We then generated a combination AAV library (regions V and VIII; Fig. 2*D*), which carries the lead epitope from the evolved region V library and a randomized region VIII. Interestingly, subjecting this library to directed evolution yielded the wild-type (WT) AAV1 sequence in region VIII (92.27%), i.e., STDPATGDVH (Fig. 2*H*). Although a second variant with the sequence DLDPKATEVE was also enriched (by 1.4%) (Fig. 2*D*), this observation demonstrates the evolutionary and structural constraints imposed by the interaction between region V and regions VIII to maintain capsid integrity. Nevertheless, these results corroborate the notion that antigenic footprints on the AAV capsid surface are mutable and can be evolved into distinct footprints while maintaining infectivity.

Individually Evolved AAV CAM Variants Retain Biochemical and Biophysical Properties of the Parental AAV1 Serotype. Multiple evolved AAV variants were selected from each library (annotated with the abbreviation CAM) for subsequent characterization. Specifically, the different variants were CAM101-107 (region IV), CAM108 (region V), and CAM109-116 (region VIII). All CAM variants packaging the ssCBA-Luc genome were produced and their transduction efficiencies assessed in vascular endothelial cells (Fig. S2*J*). A single CAM variant from each evolved library that displayed the highest transduction efficiency was shortlisted for further characterization. Specifically, CAM106 (456-SERR-459), CAM108 (492-TPGGNATR-499), and CAM109 (588-TADHDTKGVL-597) showed similar to modestly improved transduction efficiency compared with parental AAV1 on vascular endothelial cells. These observations support the notion that antigenic footprints can be reengineered and evolved while maintaining or improving on the endogenous attributes of the corresponding parental AAV strain. Further evaluation of the physical properties of these lead CAM variants confirmed that yield (vector genome titers), capsid morphology (EM), and packaging efficiency (proportion of full to empty particles) were comparable to those of parental AAV1 vectors (Fig. S2 *A*–*D*).

Individual CAM Variants Evade Neutralization by mAbs. We first evaluated the ability of single-region CAM variants to avoid neutralization by mouse mAbs ADK1a, 4E4, and 5H7 described earlier (9, 10). The three mAbs that we selected for these studies were generated from mice immunized with AAV1 (6, 17). All three mAbs bind to threefold protrusions on the capsid surface (8, 9). An earlier study showed that 4E4 and 5H7 reduce AAV1 transduction by affecting both the binding and postattachment steps essential for host cell transduction (6). As shown in Fig. 3 *A*–*C*, each CAM variant shows a distinct NAb evasion profile. As expected, parental AAV1 was neutralized by all mAbs tested at different dilutions. The CAM106 and CAM108 variants were resistant to neutralization by 4E4, whereas CAM109 was completely neutralized, similar to AAV1 (Fig. 3*A*). These observations are consistent with the observation that 4E4 maps over regions IV and V, whereas region VIII is located farther away from the capsid surface. We next determined that CAM108 and CAM109 both avoided neutralization by 5H7 (which maps over regions V and VIII), whereas CAM106 was significantly affected by 5H7, similar to AAV1 (Fig. 3*B*). With ADK1a, which partially recognizes residues within region IV at the top of the threefold protrusions, CAM106 was significantly resistant to neutralization, whereas both CAM108 and CAM109 were effectively neutralized (Fig. 3*C*).

In Vivo Neutralization Profile of CAM Variants Against mAbs. To further test whether the ability of CAM variants to avoid neutralization can be reproduced in vivo, AAV1 and CAM variants packaging ssCBA-Luc were mixed with the corresponding mAbs and injected i.m. into mice. In the absence of mAbs, all CAM variants and AAV1 showed similar luciferase transgene expression in mouse muscle (Fig. 3*E*). In the presence of antibodies, the neutralization profiles of the CAM variants corroborated the results from in vitro studies. In brief, CAM106 was resistant to ADK1a and 4E4, whereas CAM108 efficiently transduced mouse muscle in the presence of 4E4 or 5H7, and CAM109 evaded 5H7 with high efficiency. Importantly, AAV1 transduction of mouse muscle was completely abolished when coadministered with any of these antibodies (Fig. 3 *F*–*H*). Quantitative analysis of luciferase transgene expression by CAM variants normalized to AAV1 confirmed these observations (Fig. 3*I*).

Iterative Engineering of Complex Antigenic Footprints on Single-Region CAM Variants. Based on the promising results from our mAb neutralization studies, we hypothesized that combining different, evolved antigenic footprints will alter the capsid surface sufficiently to prevent recognition and neutralization by antibodies. To test this hypothesis, we generated three variants through a combination of rational mutagenesis, library generation, and iterative evolution. First, we observed that rational combination of antigenic footprints from CAM106 (region IV) and CAM108 (region V) yielded a functional and stable AAV variant, dubbed CAM117 (region IV + V) (Fig. 4*A*), but specific amino acid residues on CAM108 (region V) and CAM109 (region VIII) were not structurally compatible when combined on the same capsid. This observation is consistent with findings reported in other AAV libraries (18), in which simultaneous mutagenesis of these epitopes on the same capsid reduced viral titers, presumably owing to assembly defects. However, it is important to note that this apparent drawback can be addressed effectively by our iterative approach. Specifically, to facilitate structural compatibility, we generated an AAV capsid library on region VIII using CAM108 (region V) as a template. After three iterative cycles of directed evolution on vascular endothelial cells as described earlier, several viable variants were generated (Fig. 4*A*). After initial characterization, CAM125 (region V, 492-TPGGNATR-499; region VIII, 588-DLDPKATEVE-597) was selected for further analysis. We then iteratively engineered a third variant (CAM130) by grafting the evolved antigenic footprint from CAM106 onto CAM125. The CAM130 variant contains the following amino acid residues in three distinct antigenic footprints: region IV, 456-SERR-459; region V, 492-TPGGNATR-499; and region VIII, 588-DLDPKATEVE-597 (Fig. 4*A*). All three iteratively engineered variants—CAM117, CAM125, and CAM130—show physical attributes comparable to those of parental AAV1 with regard to vector titers and ratio of full to empty particles (Fig. S2 *D*–*I*).

CAM117, CAM 125, and CAM130 Evade Neutralizing Antisera from Preimmunized Mice. To test whether antigenically distinct CAM variants can evade polyclonal NAbs found in serum, we seroconverted mice by immunization with WT AAV1 capsids. Overall, antisera obtained from individual mice efficiently neutralized parental AAV1, whereas CAM117, CAM125, and CAM130 displayed increased resistance to neutralization (Fig. 4 *B*–*D*). In brief, we tested antisera dilutions ranging over two orders of magnitude (1:3,200–1:50) to generate sigmoidal neutralization curves. The serum concentration required for 50% neutralization of transduction (ND_{50}) was 2- to 16-fold higher for each CAM variant compared with parental AAV1 in each individual subject (Figs. 4 *B*–*D*). Furthermore, we observed an incremental ability to evade NAbs with each iterative engineering/evolution step. Specifically, the most antigenically distinct variant, CAM130, showed an 8- to 16-fold improvement in resistance to neutralization (ND_{50} >1:200; Fig. 4 *B*–*D*). These results corroborate the idea that antigenic footprints on AAV capsids are modular and cumulative in their ability to mediate NAb evasion. A similar, but less robust trend was observed with regard to the neutralizing potential of serum obtained from naïve mice used as a control (Fig. 4*E*).

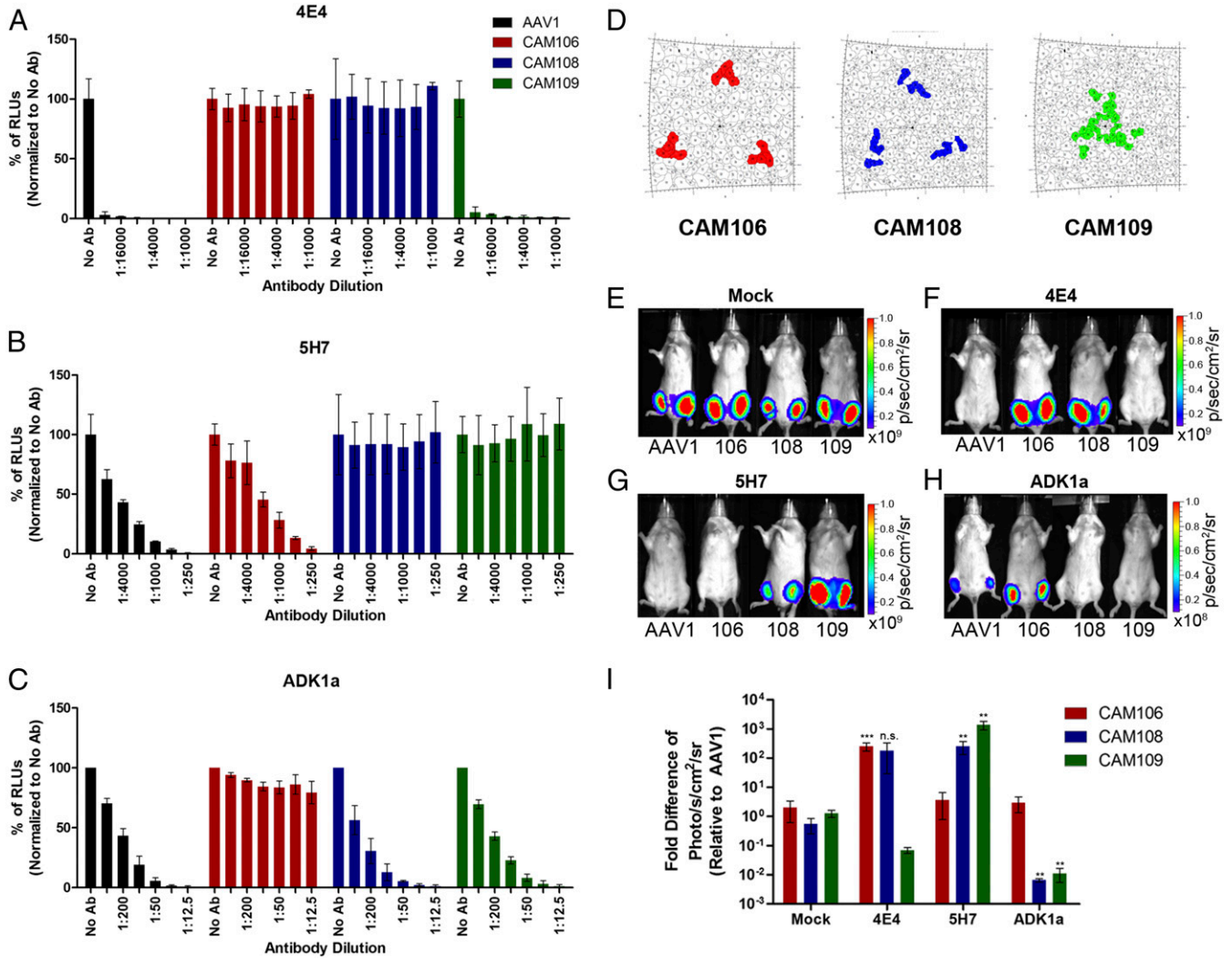

Fig. 3. Neutralization profile of AAV1 and single region CAM variants against mouse mAbs in vitro and in vivo. (*A–C*) Different AAV strains, AAV1 (black bars), CAM106 (red bars), CAM108 (blue bars), and CAM109 (green bars) evaluated against mAbs 4E4, 5H7, and ADK1a in HEK293 cells in vitro (1,000 vg/cell) at different dilutions of hybridoma media. Relative luciferase transgene expression mediated by different vectors mixed with mAbs was normalized to no-antibody controls. Error bars represent SD ($n = 4$). (*D*) Roadmap images of the threefold axis of each CAM mutant showing the location of newly evolved antigenic footprints: CAM106 (red), CAM108 (blue), and CAM109 (green). (*E–H*) Luciferase expression in mouse hindlimb muscles injected with a dose of 2×10^{10} vg of AAV1, CAM106, CAM108, and CAM109 vectors packaging ssCBA-Luc and mixed with different mAbs. Representative live animal images at 4 wk postinjection are shown in the following subgroups: no- antibody control (*E*), 4E4 (1:500) (*F*), 5H7 (1:50) (*G*), and ADK1a (1:5) (*H*). (*I*) Quantitation of luciferase activity mediated by different CAM variants relative to parental AAV1. Luciferase activity is expressed as photons/s/cm^2/sr as calculated with Living Image 3.2 software. Error bars represent SD ($n = 3$).

CAM130 Efficiently Evades Neutralization by NHP Antisera. To validate whether our approach can be translated in larger animal models, we tested the ability of AAV1 and the lead variant, CAM130, to evade NAbs generated in NHPs (rhesus macaques). In brief, we subjected AAV vectors to neutralization assays using sera collected at three different time points: preimmunization (naïve) and 4 wk and 9 wk postimmunization. All macaques seroconverted after immunization with NAb titers at the highest levels in week 4, with declines at week 9 in subjects 1 and 2 and increased potency at week 9 in subject 3 (Fig. 5). Moreover, naïve sera from subjects 1 and 3 before immunization could neutralize AAV1 effectively (Fig. 5 *A* and *G*). Because AAV1 was first identified as a contaminant in simian adenovirus stocks isolated from NHP tissue, we expected the natural host (i.e., rhesus macaques) to harbor antibodies against AAV1 capsids (19). We tested antisera dilutions ranging over two orders of magnitude (1:320–1:5) to generate neutralization curves as described earlier. Antisera obtained at 4 wk after immunization neutralized AAV1 effectively at ND_{50} >1:320. In contrast, CAM130 displayed a significant shift consistent with improved resistance to neutralization (by approximately eightfold; ND_{50} >1:40) compared with AAV1 (Fig. 5 *B*, *E*, and *H*). A similar trend toward enhanced resistance to NAbs was observed for CAM130 when evaluating antisera obtained at 9 wk postimmunization (Fig. 5 *C*, *F*, and *I*). These results strongly support the idea that antigenicity of AAV capsids can be engineered to broadly evade NAbs from different animal species on the basis of structural cues obtained from mouse mAb footprints.

CAM130 Efficiently Evades NAbs in NHP and Human Sera. To test whether CAM130 can evade NAbs and display a better profile compared with AAV1 in the general NHP and human populations, we tested serum samples obtained from cohorts of 10 subjects each. We evaluated a fixed serum dilution of 1:5 to reflect the currently mandated exclusion criterion used in ongoing clinical trials for

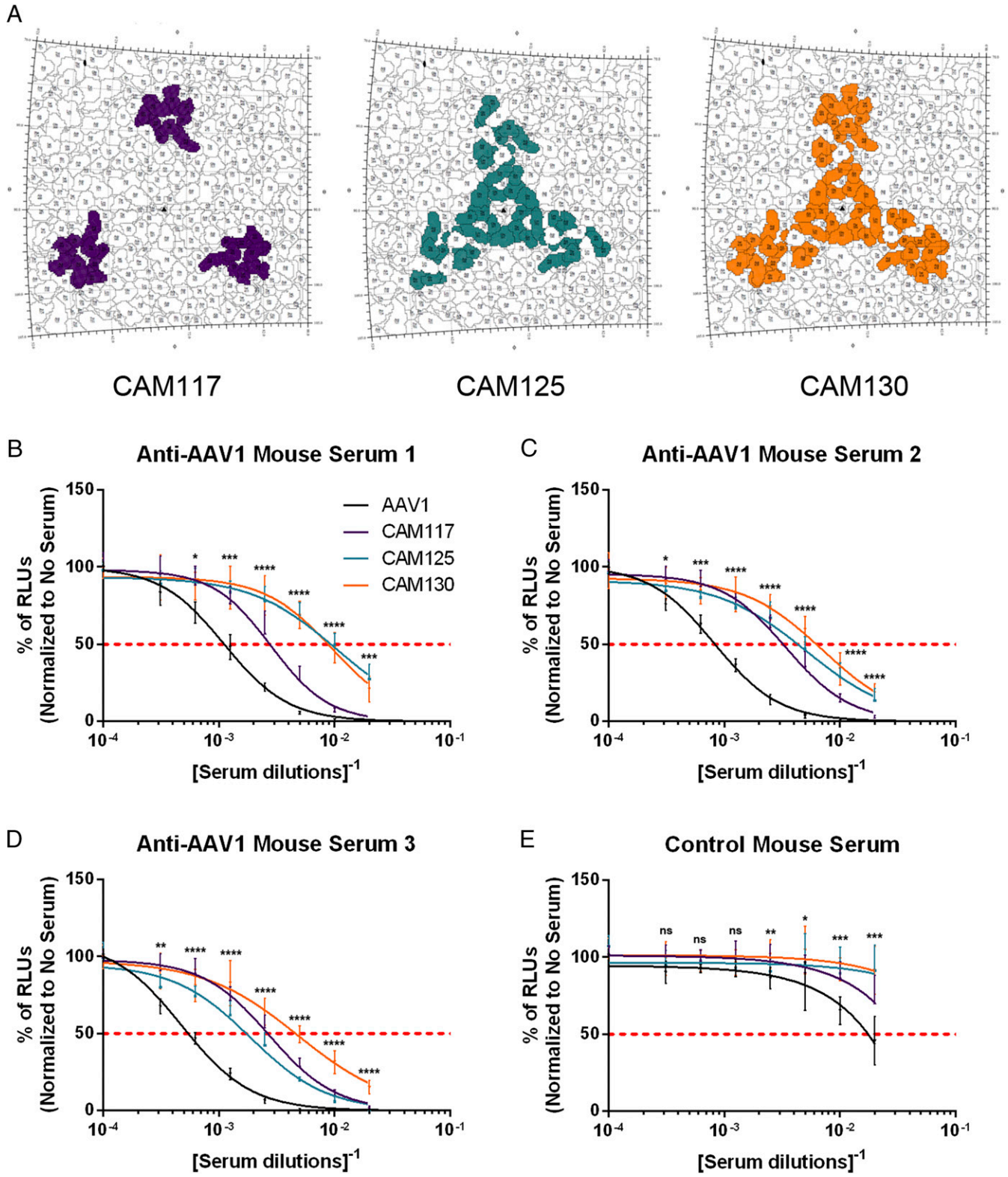

Fig. 4. Neutralization profiles of AAV1 and CAM variants in preimmunized mouse antisera. (*A*) Roadmap images of each antigenically distinct CAM variant showing newly evolved footprints at the threefold symmetry axis: CAM117 (regions IV + V, purple), CAM125 (regions V + VIII, cyan) and CAM130 (regions IV + V + VIII, orange). (*B–E*) Anti-AAV1 mouse serum from three individual animals (*B–D*) and control mouse serum (*E*) were serially diluted in twofold increments from 1:50 to 1:3,200 and then coincubated with AAV vectors in vitro (5,000 vg/cell). The dotted red line represents NAb-mediated inhibition of AAV transduction by 50%. Solid lines represent relative transduction efficiencies of AAV1 (black), CAM117 (purple), CAM125 (cyan), and CAM130 (orange) at different dilutions of antisera. Error bars represent SD (n = 3).

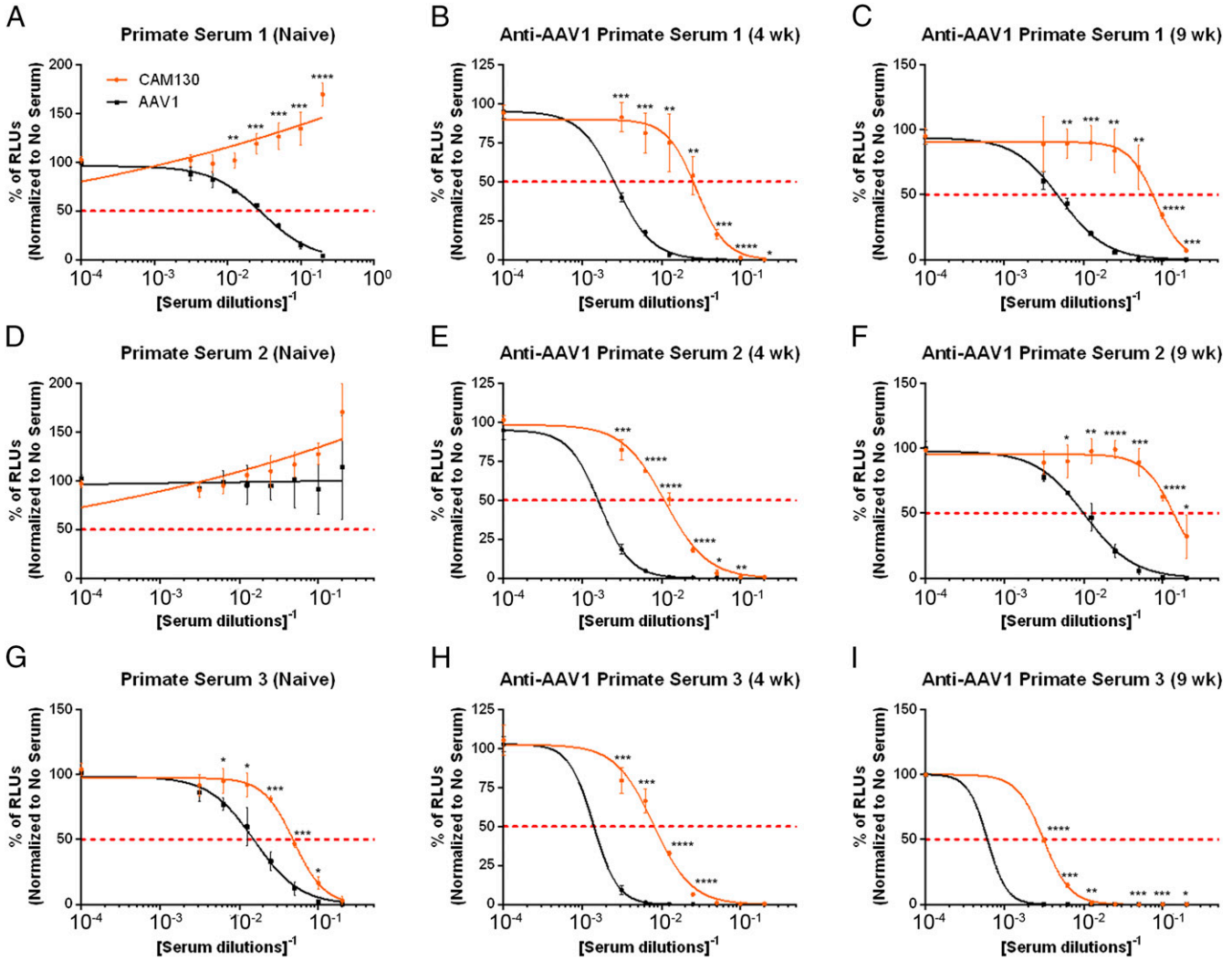

Fig. 5. Neutralization profiles of AAV1 and CAM130 in NHP antisera. Serum samples collected from three individual rhesus macaques collected preimmunization (naïve) and postimmunization (at 4 wk and 9 wk) were serially diluted in twofold increments from 1:5 to 1:320 and coincubated with AAV vectors in vitro (10,000 vg/cell). (*A*) Primate serum 1 (naïve). (*B*) Anti-AAV primate serum 1 (4 wk). (*C*) Anti-AAV primate serum 1 (9 wk). (*D*) Primate serum 2 (naïve). (*E*) Anti-AAV primate serum 2 (4 wk). (*F*) Anti-AAV primate serum 2 (9 wk). (*G*) Primate serum 3 (naïve). (*H*) Anti-AAV primate serum 3 (4 wk). (*I*) Anti-AAV primate serum 3 (9 wk). The dotted red line represents NAb-mediated inhibition of AAV transduction by 50%. Solid lines represent relative transduction efficiencies of AAV1 (black) and CAM130 (orange) at different dilutions of antisera. Error bars represent SD ($n = 3$).

hemophilia and other indications requiring systemic AAV administration. As shown in Fig. 6*A*, serum from NHP subjects p-A and p-B displayed high NAb titers that completely neutralized AAV1 and CAM130. At the other end of the spectrum, serum samples p-I and p-J neutralized neither AAV1 nor CAM130. Serum samples for subjects p-C–p-H efficiently neutralized AAV1 and reduced transduction efficiency to below 50% of that of untreated controls. None of these serum samples neutralized the antigenically distinct CAM130 variant. Thus, CAM130 showed exceptional NAb evasion in this cohort by evading 8 out of 10 serum samples (Fig. 6*A*).

We then used a similar approach to test serum from 10 human subjects using exclusion criteria (from 1:5 dilution to any detectable NAbs) mandated by several clinical gene therapy trials (e.g., ClinicalTrials.gov NCT01620801, NCT02618915, NCT01687608). We segregated human sera into two high-titer (h-A and h-B), six intermediate-titer (h-C–h-H) and two modest-titer subgroups. CAM130 was able to evade polyclonal NAbs in human sera in 8 of the 10 samples tested, whereas AAV1 did so in only 2 of the 10 samples (Fig. 6*B*). Taken together, our findings studies strongly support the idea that the three murine epitopes engineered in this study are conserved across species, and that the antigenically distinct CAM130 variant has the potential to evade antisera in a species-independent manner. Thus, our approach provides a roadmap for clinical translation and has the potential to significantly expand the patient cohort.

Antibody Evading AAV Variants Can Be Evolved Without Altering the Transduction Profile in Vivo. We compared the in vivo tissue tropism, transduction efficiency, and biodistribution of CAM130 and the parental AAV1 strain in mice. A dose of 1×10^{11} vector genomes (vg)/mouse of AAV vectors packaging scCBh-GFP was injected i.v. into 6- to 8-wk-old female BALB/c mice via the tail vein. At 3 wk postinjection, CAM130 had an apparently enhanced cardiac GFP expression profile compared with AAV1 (Fig. S3 *A* and *B*). A modest yet significant (approximately twofold) increase in GFP-positive cardiac myofibers was found in CAM130-treated animals compared with the AAV1 cohort (Fig. S3*G*). However, when we administered 1×10^{11} vg of AAV vectors packaging ssCBA-Luc genomes i.v., the increase in luciferase activity within the heart

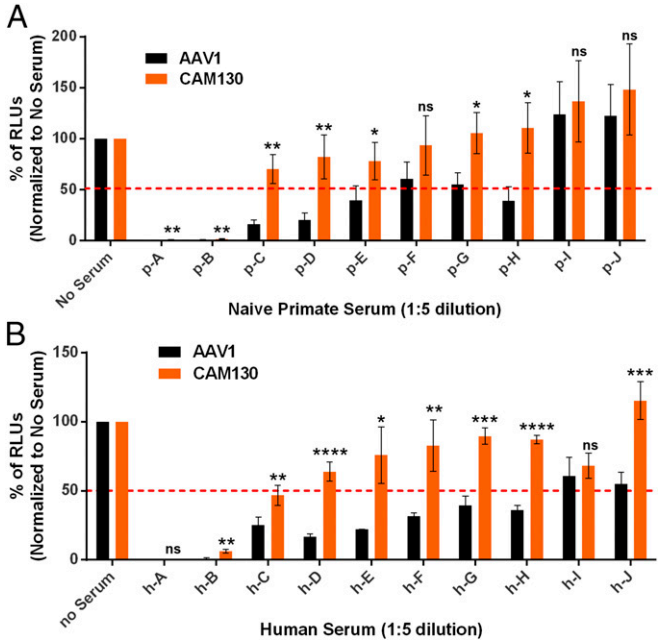

Fig. 6. Neutralization profile of AAV1 and CAM130 against individual NHP and human serum samples. AAV1 and CAM130 packaging ssCBA-Luc (10,000 vg/cell) were tested against NHP (*A*) and human (*B*) sera at 1:5 dilution to reflect clinically relevant exclusion criteria. The dotted red line represents NAb-mediated inhibition of AAV transduction by 50%. Bars represent relative transduction efficiencies of AAV1 (black) and CAM130 (orange). Error bars represent SD ($n = 3$).

compared with that seen in AAV1-treated mice was marginal and not statistically significant (Fig. S3*H*). Thus, we conclude that the CAM130 variant is as effective, if not slightly more effective, than the parental AAV1 strain. We found no major differences in transduction efficiency in other organs, including liver, lung, brain, kidney, and spleen (Fig. S4*A*). Importantly, we found no differences in the systemic biodistribution of CAM130 and AAV1 vectors in major tissues, such as heart and liver (Fig. S4*B*). In general, higher vector genome copy numbers (~10-fold) were recovered from the liver compared with cardiac tissue for both CAM130 and AAV1 vectors (Fig. S4*B*).

To further compare the tropism of CAM130 and AAV1, we evaluated the transduction profiles of these two strains after CNS administration. A dose of 3×10^9 vg of AAV1 or CAM130 packaging scCBh-GFP genomes were injected by intra-CSF administration in neonatal mice. Both AAV1 and CAM130 spread well within the brain, with a general preference for transducing the ipsilateral side more readily than the contralateral side (Fig. S3 *C* and *D*). As seen with cardiac tissue, a similar number of GFP-positive neurons was observed for CAM130 compared with AAV1 (Fig. S3*I*). In particular, CAM130 appeared to selectively transduce neurons particularly within the motor cortex, cortex, and, most prominently, in the hippocampus, similar to AAV1 (Figs. S3 *E* and *F*). Taken together, these in vivo results confirm that antigenic footprints on AAV capsids can be engineered to effectively evade NAbs without compromising vector yield, cellular/tissue tropism, or transduction and biodistribution profiles. We expect that this approach can be readily extended to other AAV serotypes as well.

Discussion

Our present study hinges on the finding that structural determinants of AAV capsid recognition by different NAbs tend to overlap and form antigenic footprints shared among different AAV isolates. In particular, a majority of antigenic determinants cluster around the threefold symmetry axes on the AAV capsid. In some cases, antigenic regions also have been mapped to the twofold to fivefold wall region on AAV capsids (8); however, it is highly likely that these antigenic footprints and other potential new sites, if identified, could be iteratively engineered onto our variants in a mutually exclusive fashion. At present, no experimental or computational approaches are available for engineering future antigenic variants of AAV before they emerge in nature. Earlier engineering strategies to address the problem of NAbs relied on the limited antigenic variability among different natural AAV isolates and yielded chimeric or ancestral AAV capsids (20–22). Complementarily, our approach explores the entire sequence space for each amino acid residue within antigenic footprints located on any AAV capsid surface. Thus, the evolved AAV-CAM variants described herein are antigenically distinct and contain synthetic antigenic footprints not existent in nature.

Early in our efforts, we observed a cumulative effect on the ability of CAM variants to evade NAbs as we grafted multiple new antigenic epitopes on the same capsid. However, not all combinations yielded viable capsids, suggesting potential structural incompatibilities when combining different engineered epitopes. To address this concern, we iteratively engineered a second-generation AAV capsid library derived from CAM variants evolved in the earlier round. This iterative approach resulted in CAM variants that can be produced at high yields, are highly potent, and demonstrate NAb evasion potential. Significantly, the antigenically distinct AAV variant CAM130 has the ability to avoid neutralization by mouse, NHP, and human antisera. These observations strongly support the idea that antigenic recognition of AAV capsids is significantly conserved across animal and human species. Although more comprehensive studies evaluating the seroprevalence of AAV CAM variants in prospective patients will be essential, the multispecies data described in this study provide a promising path forward for clinical translation.

Another important implication of our proof-of-concept study with AAV1 is that structure-guided evolution can be readily adapted to modify other AAV serotypes as well as engineered strains. A comprehensive (if not exhaustive) structural dataset is now available for mAbs complexed with different AAV serotypes (8, 9), which strongly supports the idea that antigenic determinants on different AAV serotypes are evolutionarily conserved. Given that the antigenic residues cluster predominantly into overlapping footprints on the capsid surface, our approach is likely to yield antigenically distinct variants derived from any AAV capsid template.

A critical aspect of our approach is that antigenic epitopes on the AAV capsid can be artificially evolved while maintaining endogenous functions. This finding significantly expands our knowledge of various amino acid residues that can be tolerated within antigenic footprints without affecting viral titer, infectivity, and tropism. Specifically, AAV1 requires sialylated glycans for cell surface attachment, which in turn determines transduction efficiency (23). The SA-binding site of AAV1 was resolved recently, revealing specific contact residues located in a pocket at the base of the threefold protrusions similar to the galactose binding site on AAV9 (16). Specific residues located within the SA binding pocket include S268, D270, N271, N447, S472, V473, N500, T502, and W503. The present study was designed to avoid manipulation of these residues owing to their involvement with SA binding and partial overlap with the region encoding the assembly-activating protein in the WT AAV genome (24). Although we cannot rule out the possibility that the newly evolved antigenic epitopes on the AAV CAM variants alter SA binding or, consequently, the infectious pathway(s) of parental AAV1, it is important to note that our approach ensures that yield or transduction efficiency is not adversely impacted. Further analysis of the 3D structure of AAV CAM variants, their receptor use, and infectious pathway(s) are likely

to shed more light on structure-function correlates of AAV CAM variants and guide future clinical applications.

This proof-of-principle study suggests that CAM variants have the potential for use in patients with anti-AAV NAbs arising due to natural exposure or previous treatment with recombinant vectors based on natural AAV serotypes. However, the exact clinical implications of the approximate log-order increase in resistance to NAbs by CAM130 compared with AAV1 remain unclear. In this regard, the next steps will involve characterization of the immune profile of CAM130 in a large cohort of patient serum samples, along with dose-finding studies in large animal models.

It is also important to acknowledge that the newly evolved capsid variants likely will elicit a different subset of NAbs on injection, limiting repeated administration. Although CAM variants can be reengineered further, if warranted, our structure-guided approach complements other methods to circumvent preexisting humoral immunity in prospective patients that are currently being explored in preclinical studies (5). One promising approach involves the use of immunosuppressive agents that can mitigate NAb generation after vector dosing (25). Although the side effects of these agents are well documented, this approach may help develop treatment regimens that require vector redosing. Studies also have demonstrated that several rounds of plasmapheresis can lower NAb titers from high to medium levels (as low as 1:20) in patients (26, 27); however, this approach does not appear to be as effective in further reducing medium-to-low NAb titers that preclude patient enrollment (27). Nevertheless, combined use of plasmapheresis and antibody-evading CAM variants in prospective patients with high NAb titers may effectively address this challenge. Overall, our structure-guided approach demonstrates the potential to make gene therapy, silencing, and/or editing modalities with recombinant AAV vectors available to an expanded patient cohort.

Materials and Methods

Cells, Viruses, and Antibodies. HEK293 and MB114 cells (a kind gift from Linda Van Dyk, University of Colorado) were maintained in DMEM supplemented with 10% FBS (Thermo Fisher Scientific), 100 U/mL penicillin, and 10 μg/mL streptomycin (Thermo Fisher Scientific) in 5% CO_2 at 37 °C. Murine adenovirus 1 (MAV-1) was purchased from American Type Culture Collection and amplified by infecting MB114 cells at a multiplicity of infection (MOI) of 1. At day 6 postinfection (~50% cytopathic effect), media containing progeny MAV-1 viruses were harvested and centrifuged at 3,000 × *g* for 5 min, and the supernatant was stored at −80 °C for subsequent evolution studies. Mouse anti-AAV1 mAbs ADK1a, 4E4, and 5H7 have been described previously (6, 9, 17). Naïve human serum samples were purchased from Valley Biomedical. Naïve serum from rhesus macaques was a kind gift from Yoland Smith and Adriana Galvan (Yerkes National Primate Center, Emory University). Antisera against AAV1 capsids, generated by immunizing rhesus macaques i.m. with AAV1 capsids, was a kind gift from Jonah Sacha (Oregon National Primate Center). All mouse, human, and NHP sera used in this study were heat-inactivated at 55 °C for 15 min before use.

Recombinant AAV Production, Purification, and Quantification. Recombinant AAV vectors were produced by transfecting four 150-mm dishes containing HEK293 cells at 70–80% confluence with polyethylenimine using the triple-plasmid protocol. Recombinant vectors packaging single-stranded genomes encoding firefly luciferase driven by the chicken β-actin promoter (ssCBA-Luc) or self-complementary green fluorescence protein driven by a hybrid chicken β-actin promoter (scCBh-GFP) were generated using this method. Subsequent steps involving the harvesting of recombinant AAV vectors and downstream purification were carried out using updated methods (28). Recombinant AAV vector titers were determined by quantitative PCR with primers amplifying AAV2 inverted terminal repeat regions, 5′-AACATGCTACGCAGAGAGGGAGTGG-3′ and 5′-CATGAGACAAGGAACCCCTAGTGATGGAG-3′.

Structural Modeling and Analysis of AAV Antigenic Footprints. Antigenic footprints of AAV serotypes 1/6, AAV2, AAV5, and AAV8 were determined using previously resolved structures of AAV capsids complexed with different mouse mAbs (8, 9). To restrict diversity and maximize the efficiency of AAV library generation, only amino acid residues directly in contact with antibodies were included for analysis. Contact surface residues on each serotype were either aligned by Clustal Omega or structurally superimposed using PyMOL (Schrödinger). Structural alignment revealed that antibody footprints from multiple serotypes overlap in close proximity to the threefold symmetry axis or around the fivefold pore and close to the twofold depression, especially at the twofold or fivefold wall (8, 9). Of these CAMs, we determined that the majority of the antibodies analyzed have direct contact with the threefold symmetry or the twofold or fivefold wall, supporting the notion that these regions are critical antigenic determinants on the AAV capsid (8, 9). For the present study, antigenic footprints for three distinct mAbs (4E4, 5H7, and ADK1a) were visualized on the AAV1 capsid (Protein Data Bank ID code 3NG9), and roadmap images were generated using RIVEM (29).

Generation of AAV Capsid Libraries. AAV libraries were engineered through saturation mutagenesis of amino acid residues within different antigenic footprints associated with distinct mAbs described above. In brief, for Gibson assembly, 12 oligos with an average length of 70 nt were ordered from IDT. Each oligo contained at least 15–20 nt overlapping homology to the neighboring oligos. Three oligos contained degenerate nucleotides within genomic regions coding for different antigenic footprints. Plasmid libraries were then generated by in vitro assembly of multiple oligos using High-Fidelity Gibson Assembly Mix (New England BioLabs) according to the manufacturer's instructions. The assembled fragments were either PCR-amplified for 10 cycles using Phusion HF (New England BioLabs) or directly cloned into pTR-AAV1** plasmid between the BspEI and SbfI restriction sites. Plasmid pTR-AAV1** contains genes encoding AAV2 Rep and AAV1 Cap with stop codons at positions 490 and 491 (AAV1 VP1 numbering) introduced by site-directed mutagenesis (Agilent). The entire construct is flanked by AAV2 inverted terminal repeats to enable packaging and replication of pseudotyped AAV1 libraries on helper virus coinfection. Of note, the AAV1** capsid gene was incorporated before library cloning, to reduce WT AAV1 plasmid contamination during cloning. Ligation reactions were then concentrated and purified by ethanol precipitation. Purified ligation products were electroporated into DH10B ElectroMax cells (Invitrogen) and directly plated on multiple 5,245-mm^2 bioassay dishes (Corning) to avoid bias from bacterial suspension cultures. Plasmid DNA from pTR-AAV1CAM libraries were purified from pooled colonies grown on LB agar plates using the Invitrogen Maxiprep Kit.

Evolution of AAV CAM Strains. Equal amounts (15 μg) of each pTR-AAV1CAM library and the Ad helper plasmid pXX680 were transfected onto HEK293 cells at 70–80% confluency on each 150-mm dish using polyethylenimine to generate CAM viral libraries. AAV CAM libraries were purified using standard procedures described earlier. MB114 cells were seeded on a 150-mm tissue culture dish overnight to reach 60–70% confluence before inoculation with AAV CAM libraries at an MOI ranging from 1,000 to 10,000. At 24 h posttransduction, MAV-1 was added as a helper virus to promote AAV replication. At 6 d postinfection with MAV-1 (50% cytopathic effect), the supernatant was harvested, and DNase I-resistant vector genomes were quantified on day 7. Media containing replicating AAV strains and MAV-1 obtained from each round of infection were then used as inoculum for each subsequent cycle, for a total of five rounds of evolution. Subsequent iterative rounds of evolution were carried out in a similar fashion with AAV capsid libraries containing different permutations and combinations of newly evolved antigenic footprints.

Identification of Newly Evolved AAV Strains. To analyze the sequence diversity of the parental and evolved AAV CAM libraries, DNase I resistant vector genomes were isolated from media and amplified by Q5 polymerase for 10–18 cycles (New England BioLabs) using primers 5′-CCCTACACGACGCTCTTCCGATCTNNNNNcagaactcaaaatcagtccggaagt-3′ and 5′-GACTGGAGTTCAGACGTGTGCTCTTCCGATCTNNNNNgccaggtaatgctcccatagc-3′. Illumina MiSeq sequencing adaptor for multiplexing was added in a second round of PCR using Q5 Polymerase with P5 and P7 primers. After each round of PCR, the products were purified using the PureLink PCR Micro Kit (Thermo Fisher Scientific). The quality of the amplicons was verified using a Bioanalyzer (Agilent), and concentrations were quantified using a Qubit spectrometer (Thermo Fisher Scientific). Libraries were then prepared for sequencing with the Illumina MiSeq 300 Reagent Kit v2, following the manufacturer's instructions, and sequenced on the MiSeq system.

Sequencing Data Analysis. Demultiplexed reads were subjected to a quality control check using FastQC (v.0.11.5), with no sequences flagged for poor

quality, and analyzed via a custom Perl script (Dataset S1). In brief, raw sequencing files were probed for mutagenized regions of interest, and the frequencies of different nucleotide sequences in this region were counted and ranked for each library. Nucleotide sequences were also translated, and these amino acid sequences were similarly counted and ranked. Amino acid sequence frequencies across libraries were then plotted in the R graphics package v3.2.4.

Isolation of AAV CAM Variants for Characterization. To characterize selected clones from each library, DNase I-resistant vector genomes were isolated from media and amplified by Phusion HF (New England BioLabs) using primers flanking the BspEI and SbfI sites. The PCR products were gel-purified, subcloned into TOPO cloning vectors (Thermo Fisher Scientific), and sent out for standard Sanger sequencing (Eton Bioscience). Unique sequences were subcloned into an AAV helper plasmid backbone using BspEI and SbfI sites. Unique recombinant AAV CAM variants were produced following an updated AAV vector production protocol (28).

In Vitro Antibody and Serum Neutralization Assays. Here 25 μL of antibody or antiserum (as specified for individual experiments) was mixed with an equal volume containing recombinant AAV vectors (1,000-10,000 vg/cell) in tissue culture-treated, black, glass- bottom 96-well plates (Corning) and then incubated at room temperature for 30 min. Assay parameters were carefully controlled as outlined previously (30). A total of 5×10^4 HEK293 cells in 50 μL of medium was then added to each well, and the plates were incubated in 5% CO_2 at 37 °C for 48 h. Cells were then lysed with 25 μL of 1× passive lysis buffer (Promega) for 30 min at room temperature. Luciferase activity was measured on a Victor 3 multilabel plate reader (PerkinElmer) immediately after the addition of 25 μL of luciferin (Promega). All readouts were normalized to controls with no antibody/antiserum treatment. Recombinant AAV vectors packaging ssCBA-Luc transgenes were prediluted in DMEM + 5% FBS + penicillin-streptomycin and used in this assay.

In Vivo Antibody Neutralization Assay. Each hind limb of 6- to 8-wk-old female BALB/c mice (Jackson Laboratory) was injected i.m. with 2×10^{10} AAV packaging CBA-Luc premixed with three different mAbs—4E4, 5H7, and ADK1a—at 1:500, 1:50, and 1:5 dilution, respectively, in a final volume of 20 μL. At 4 wk postinjection, luciferase activity was measured using a Xenogen IVIS Lumina system (PerkinElmer) at 5 min after i.p. injection of 175 μL of in vivo D-luciferin (120 mg/kg; Nanolight) per mouse. Luciferase activity was measured as photons/s/cm^2/sr and analyzed using Living Image 3.2 software (Caliper Life Sciences).

Statistical Analysis. Statistical analysis was carried out with GraphPad Prism software using an unpaired, two-tailed Student *t* test. In the figures, $*P < 0.5$, $**P < 0.05$, $***P < 0.005$, $****P < 0.0005$, n.s. means not significant, and error bars represent 1 SD.

ACKNOWLEDGMENTS. We thank Giridhar Murlidharan, Rita Meganck, Rebecca Reardon, Lavanya Rao, and Travis Corriher for their technical help, as well as Drs. Benjamin Burwitz, Jonah Sacha, Yoland Smith, and Adriana Galvan for providing NHP serum samples. This work was supported by National Institutes of Health Grants P01 HL112761 and R01 HL089221 (to A.A.), a Ruth L. Kirschstein National Research Service Award postdoctoral fellowship (to R.M.C.R.), Grant R01 GM082946 (to M.A.-M.), and Grant T32-GM008799 (to J.K.S.).

1. Ledford H (2015) Success against blindness encourages gene therapy researchers. *Nature* 526:487–488.
2. Nienhuis AW, Nathwani AC, Davidoff AM (2016) Gene therapy for hemophilia. *Hum Gene Ther* 27:305–308.
3. Hastie E, Samulski RJ (2015) Adeno-associated virus at 50: A golden anniversary of discovery, research, and gene therapy success—a personal perspective. *Hum Gene Ther* 26:257–265.
4. Greenberg B, et al. (2016) Prevalence of AAV1 neutralizing antibodies and consequences for a clinical trial of gene transfer for advanced heart failure. *Gene Ther* 23: 313–319.
5. Tse LV, Moller-Tank S, Asokan A (2015) Strategies to circumvent humoral immunity to adeno-associated viral vectors. *Expert Opin Biol Ther* 15:845–855.
6. Harbison CE, et al. (2012) Examining the cross-reactivity and neutralization mechanisms of a panel of mAbs against adeno-associated virus serotypes 1 and 5. *J Gen Virol* 93:347–355.
7. Berns KI, Muzyczka N (2017) AAV: An overview of unanswered questions. *Hum Gene Ther* 28:308–313.
8. Tseng YS, Agbandje-McKenna M (2014) Mapping the AAV capsid host antibody response toward the development of second-generation gene delivery vectors. *Front Immunol* 5:9.
9. Tseng YS, et al. (2015) Adeno-associated virus serotype 1 (AAV1)- and AAV5-antibody complex structures reveal evolutionary commonalities in parvovirus antigenic reactivity. *J Virol* 89:1794–1808.
10. Gurda BL, et al. (2013) Capsid antibodies to different adeno-associated virus serotypes bind common regions. *J Virol* 87:9111–9124.
11. Gurda BL, et al. (2012) Mapping a neutralizing epitope onto the capsid of adeno-associated virus serotype 8. *J Virol* 86:7739–7751.
12. McCraw DM, O'Donnell JK, Taylor KA, Stagg SM, Chapman MS (2012) Structure of adeno-associated virus-2 in complex with neutralizing monoclonal antibody A20. *Virology* 431:40–49.
13. Bloom ME, et al. (2001) Identification of Aleutian mink disease parvovirus capsid sequences mediating antibody-dependent enhancement of infection, virus neutralization, and immune complex formation. *J Virol* 75:11116–11127.
14. Wikoff WR, et al. (1994) The structure of a neutralized virus: Canine parvovirus complexed with neutralizing antibody fragment. *Structure* 2:595–607.
15. Hafenstein S, et al. (2009) Structural comparison of different antibodies interacting with parvovirus capsids. *J Virol* 83:5556–5566.
16. Huang LY, et al. (2016) Characterization of the adeno-associated virus 1 and 6 sialic acid binding site. *J Virol* 90:5219–5230.
17. Kuck D, Kern A, Kleinschmidt JA (2007) Development of AAV serotype-specific ELISAs using novel monoclonal antibodies. *J Virol Methods* 140:17–24.
18. Marsic D, et al. (2014) Vector design tour de force: Integrating combinatorial and rational approaches to derive novel adeno-associated virus variants. *Mol Ther* 22: 1900–1909.
19. Atchison RW, Casto BC, Hammon WM (1965) Adenovirus-associated defective virus particles. *Science* 149:754–756.
20. Santiago-Ortiz J, et al. (2015) AAV ancestral reconstruction library enables selection of broadly infectious viral variants. *Gene Ther* 22:934–946.
21. Zinn E, et al. (2015) In silico reconstruction of the viral evolutionary lineage yields a potent gene therapy vector. *Cell Reports* 12:1056–1068.
22. Kotterman MA, Schaffer DV (2014) Engineering adeno-associated viruses for clinical gene therapy. *Nat Rev Genet* 15:445–451.
23. Wu Z, Miller E, Agbandje-McKenna M, Samulski RJ (2006) α2,3 and α2,6 N-linked sialic acids facilitate efficient binding and transduction by adeno-associated virus types 1 and 6. *J Virol* 80:9093–9103.
24. Sonntag F, Schmidt K, Kleinschmidt JA (2010) A viral assembly factor promotes AAV2 capsid formation in the nucleolus. *Proc Natl Acad Sci USA* 107:10220–10225.
25. Corti M, et al. (2014) B-cell depletion is protective against Anti-AAV capsid immune response: A human subject case study. *Mol Ther Methods Clin Dev* 1:14033.
26. Chicoine LG, et al. (2014) Plasmapheresis eliminates the negative impact of AAV antibodies on microdystrophin gene expression following vascular delivery. *Mol Ther* 22:338–347.
27. Monteilhet V, et al. (2011) A 10 patient case report on the impact of plasmapheresis upon neutralizing factors against adeno-associated virus (AAV) types 1, 2, 6, and 8. *Mol Ther* 19:2084–2091.
28. Murlidharan G, et al. (2016) CNS-restricted transduction and CRISPR/Cas9-mediated gene deletion with an engineered AAV vector. *Mol Ther Nucleic Acids* 5:e338.
29. Xiao C, Rossmann MG (2007) Interpretation of electron density with stereographic roadmap projections. *J Struct Biol* 158:182–187.
30. Wang M, et al. (2015) Prediction of adeno-associated virus neutralizing antibody activity for clinical application. *Gene Ther* 22:984–992.